

MAXIMUM LIFT OF WINGS WITH LEADING-EDGE DEVICES AND TRAILING EDGE FLAPS DEPLOYED

1. NOTATION AND UNITS

		<i>SI</i>	<i>British</i>
A	aspect ratio, $2s/\bar{c}$		
C_L	lift coefficient; (lift per unit span)/ qc for aerofoil, (lift)/ qS for wing		
C_{LL}	wing local lift coefficient; (lift per unit span)/ qc		
C_{LLp}	peak (<i>i.e.</i> maximum) value of C_{LL}		
C_{Lm}	aerofoil section maximum lift coefficient		
C_{Lmax}	wing maximum lift coefficient		
C_{LmaxB}	wing maximum lift coefficient with high-lift devices undeployed (<i>i.e.</i> "basic" wing)		
ΔC_{Lm}	increment in aerofoil section maximum lift coefficient due to deployment of high-lift devices		
ΔC_{Lmaxl}	increment in wing maximum lift coefficient due to deployment of leading-edge devices		
ΔC_{Lmaxt}	increment in wing maximum lift coefficient due to deployment of trailing-edge flaps		
ΔC_{Lml}	increment in aerofoil section maximum lift coefficient due to deployment of leading-edge device, based on c ; datum value for Reynolds number of 3.5×10^6		
$\Delta C'_{Lml}$	increment in aerofoil section maximum lift coefficient due to deployment of leading-edge device, based on c' ; datum value for Reynolds number of 3.5×10^6		
c	wing local chord, see Sketch 1.1; basic aerofoil section chord	m	ft
c'	wing extended local chord	m	ft
c_{el}	effective chord of leading-edge device (see Table 4.1 of Item No. 94027)	m	ft
c_l	chord of leading-edge device (see Sketches 4.1 and 4.2 of Item No. 94027)	m	ft

Δc_l	chord extension due to deployment of leading-edge device (see Sketches 4.1 to 4.3 of Item No. 94027)	m	ft
c'_l	extended chord of leading-edge device (see Sketches 4.1 to 4.3 of Item No. 94027)	m	ft
c_p	wing chord at spanwise location of peak loading due to incidence, see Sketch 1.1	m	ft
c_r	wing root (centre-line) chord	m	ft
c_t	chord of trailing-edge flap	m	ft
Δc_t	increment in flap chord	m	ft
\bar{c}	wing geometric mean chord	m	ft
$\bar{\bar{c}}$	wing aerodynamic mean chord	m	ft
F_R	factor for effect of Reynolds number on ΔC_{Lmax} , see Equation (6.5) or (6.7)	m	ft
G_l	gap between trailing edge of deployed slat or vented Krüger flap and aerofoil surface, measured normal to aerofoil surface (see Sketches 4.2(a) and 4.2(b) of Item No. 94027)	m	ft
H_l	height of trailing edge of leading-edge device above basic aerofoil chord line (see Sketches 4.2 and 4.3 of Item No. 94027)	m	ft
K_e	correlation factor for overlap of slat trailing edge (Figure 3 of Item No. 94027)		
K_g	correlation factor for geometry of leading-edge device (Figures 2a and 2b of Item No. 94027)		
K_l	correlation factor for effect of leading-edge device deflection (Figures 1a to 1c of Item No. 94027, Figure 5 of Item No. 94030 and Figure 10 of Item No. 94031)		
$K_{\Delta l}$	correlation factor for wing sweep, see Section 6.3		
L_l	overlap between trailing edge of deployed slat or vented Krüger flap and fixed aerofoil nose (see Sketches 4.2(a) and 4.2(b) of Item No. 94027)	m	ft
M	free-stream Mach number		
q	free-stream kinetic pressure	N/m ²	lbf/ft ²
R_c	Reynolds number based on free-stream conditions and c		
$R_{\bar{c}}$	Reynolds number based on free-stream conditions and $\bar{\bar{c}}$		

S	wing planform area, $2s\bar{c}$	m^2	ft^2
s	wing semi-span	m	ft
t	maximum thickness of aerofoil	m	ft
x_l	chordwise location of undeployed slat trailing-edge (see Sketch 4.2(a) of Item No. 94027)	m	ft
x_n	chordwise position of fixed aerofoil nose (see Sketch 4.2(a) of Item No. 94027)	m	ft
β	compressibility parameter, $(1 - M^2)^{1/2}$		
δ_l, δ_l°	deflection angle of leading-edge device, measured streamwise (see Sketches 4.1 to 4.3 of Item No. 94027)	rad, deg	rad, deg
δ_t, δ_t°	deflection angle of trailing-edge flap, measured streamwise (see Sketch 4.1 of Item Nos 94028 and 94029)	rad, deg	rad, deg
η	spanwise distance from wing centre-line as fraction of semi-span		
η_{il}, η_{it}	value of η at inboard limit of leading-edge device, trailing-edge flap		
η_{ol}, η_{ot}	value of η at outboard limit of leading-edge device, trailing-edge flap		
η_p	value of η for μ_p		
$\bar{\eta}$	spanwise centre of pressure position for loading due to incidence (see Item No. 83040)		
κ	wing taper parameter in Item No. 83040; $\int_0^1 (c/\bar{c})\eta d\eta$, giving $(1 + 2\lambda)/[3(1 + \lambda)]$ for straight tapered wing		
Λ_{hl}	leading-edge device hinge-line sweep angle	deg	deg
Λ_0	wing leading-edge sweep angle, see Sketch 1.1	deg	deg
$\Lambda_{1/4}$	wing quarter-chord sweep angle	deg	deg
$\Lambda_{1/2}$	wing mid-chord sweep angle	deg	deg
Λ_1	wing trailing-edge sweep angle, see Sketch 1.1	deg	deg
λ	wing taper ratio, (tip chord)/(root chord)		
μ	normalised local lift coefficient, C_{LL}/C_L		
μ_p	peak (<i>i.e.</i> maximum) value of μ		

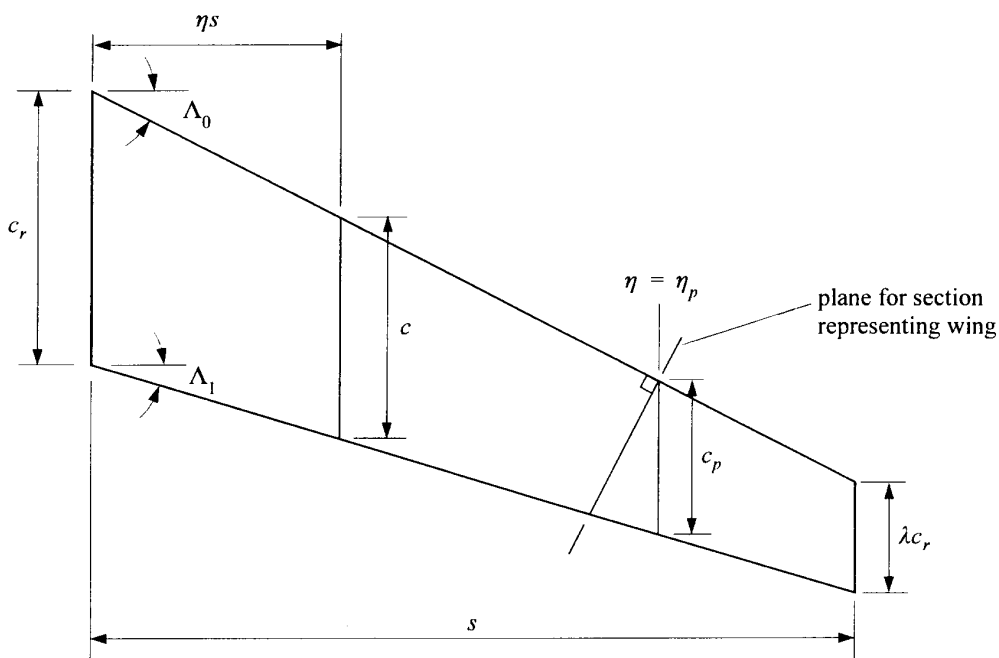
ρ_l	aerofoil leading-edge radius	m	ft
ϕ_t°	angle between basic aerofoil datum chord at trailing edge and upper surface, projected if necessary (see Sketch 4.1 of Item No. 94028)	deg	deg
ψ_i	part-span factor; lift coefficient increment due to part-span leading-edge device extending symmetrically from η_{il} out to wing tip, divided by lift coefficient increment due to full-span leading-edge device at same setting and wing angle of attack		

Subscripts

l	denotes value for leading-edge device
m	denotes aerofoil value of maximum lift
max	denotes wing value of maximum lift
p	denotes value for section at η_p
t	denotes value for trailing-edge flap
$()_{expt}$	denotes experimental value
$()_{pred}$	denotes predicted value

Superscript

$^\circ$	denotes angle in degrees
----------	--------------------------



Sketch 1.1 Wing notation

2. INTRODUCTION

In this Item the increment in maximum lift coefficient due to the deployment of leading-edge devices on a wing is derived from the increment in maximum lift coefficient due to a leading-edge device on an aerofoil section representative of the wing. For wings with full-span high-lift devices the three-dimensional effects are similar to those for a plain wing (*i.e.* a wing with or without camber or twist but without deployment of manoeuvre or high-lift devices such as leading-edge or trailing-edge flaps); separation usually starts near the most highly loaded spanwise station and spreads rapidly with increasing incidence. For this reason the basic concepts used in Item No. 89034 (Derivation 4), with regard to the importance of the spanwise loading and the relevance of the most highly loaded section, are maintained in this Item.

The methods for the prediction of aerofoil section maximum lift coefficient, C_{Lm} , and the increment to it, ΔC_{Lm} , due to deployment of leading-edge devices and trailing-edge flaps are presented respectively in Item No. 84026 (Derivation 3) and Item Nos 94026 to 94031 (Derivations 6 to 11).

The methods for the prediction of wing maximum lift coefficient, C_{LmaxB} , for a plain cambered and twisted wing, and the incremental wing maximum lift coefficient, ΔC_{Lmax} , due to deployment of trailing-edge flaps are presented respectively in Item No. 89034 and Item No. 91014 (Derivation 5). Those methods utilise the aerofoil section data of Item No. 84026 and Item Nos 94026 and 94028 to 94031.

The method of the present Item extends the scope of this series of Items by using the aerofoil section data of Item No. 94027 in the prediction of ΔC_{Lmax} , the increment in maximum lift coefficient of a wing due to the deployment of leading-edge devices. The maximum lift coefficient, ΔC_{Lmax} , of wings with leading-edge devices deployed can therefore be obtained by the use of this Item in combination with Item No. 89034.

For subsonic speeds, the increment in maximum lift coefficient due to the deployment of leading-edge devices on a high aspect ratio wing with no sweep is, to a first approximation, determined by the increment in the maximum lift coefficient due to the leading-edge high-lift devices on the aerofoil section. The main parameters which influence the increment in maximum lift coefficient due to leading-edge devices on an aerofoil section are the type of device, the effective chord, the change in chord length due to leading-edge device deployment, aerofoil section geometry, Reynolds number and Mach number. For leading-edge high-lift devices on wings additional parameters influence the increment in maximum lift coefficient, in particular aspect ratio, taper ratio, sweep and spanwise extent of the device and the presence of a trailing-edge flap. This Item has been developed in conjunction with Item No. 91014 to provide an estimation of the effects of leading-edge devices and trailing-edge flaps in combination.

Leading-edge devices are deployed on unswept wings and wings of moderate sweep ($\Lambda_0 \leq 35^\circ$) primarily so as to increase the maximum lift. Leading-edge devices work by reducing the suction on the upper surface near the leading edge of the wing, to allow an increase in angle of attack before the wing stalls. A more detailed explanation is given in Item No. 94026 and in Reference 27. In general the increased lift cannot be utilised to improve airfield performance because the resulting aircraft attitude would exceed the tail scrape angle. For this reason, for maximum lift, leading-edge devices are invariably used in combination with trailing-edge flaps. For wings of greater sweep, leading-edge devices are often used on their own or in combination with trailing-edge devices to allow greater angles of attack to be attained before outer wing flow breakdown occurs, thus alleviating premature pitch-up or wing-drop and allowing the use of greater lift coefficients. Another use is to increase the available lift before wing buffet occurs.

Experimental data for incremental maximum lift due to leading-edge devices alone are less systematic than for trailing-edge flaps. In the preparation of this Item it has been found that when it is used in combination with Item No. 91014 for trailing-edge flaps there is some improvement in the accuracy of prediction. The method is therefore best suited to the prediction of the increment in maximum lift coefficient due to leading-edge devices on wings with trailing-edge flaps also deployed.

3. REQUIRED DATA ITEMS

Other ESDU Data Items that may be required in the use of this Item are:

<i>Data Item No.</i>	<i>Derivation No.</i>	<i>For Determination of</i>
76003	1	Various geometrical relationships for wings.
83040	2	Spanwise centre of pressure location.
84026	3	Aerofoil maximum lift coefficient for $M \approx 0$.
89034	4	Maximum lift coefficient of plain wings at subsonic speeds.
91014	5	Maximum lift coefficient of wings with trailing-edge flaps at low speeds.
		Increment in aerofoil maximum lift coefficient due to deployment of:
94027	7	leading-edge devices,
94028	8	plain trailing-edge flaps,
94029	9	trailing-edge split flaps,
94030	10	single-slotted trailing-edge flaps,
94031	11	double-slotted and triple-slotted trailing-edge flaps.

4. SCOPE OF ITEM

The method of obtaining the maximum lift coefficient increment of the wing due to a leading-edge device, ΔC_{Lmaxl} , involves the evaluation of the increment $\Delta C'_{Lml}$, due to the deployment of the leading-edge device on the aerofoil section at the spanwise location of the peak loading due to incidence. The value of $\Delta C'_{Lml}$, obtained from Item No. 94027, is then factored to allow for the effects of aspect ratio, taper ratio, sweep and part-span effects. It is recommended that similar factors be applied to all leading-edge devices. The method can therefore be used for all those leading-edge devices considered in Item No. 94027, namely plain flaps, drooped leading edges, slats (including sealed slats) and Krüger flaps (including vented Krügers). The method also applies to the increment in maximum lift coefficient due to the deployment of a leading-edge device on a wing which has a trailing-edge device deployed, including any of those considered in Item No. 91014, namely, plain, split, single-, double- and triple-slotted flaps. The ranges of geometrical and flow parameters for the experimental data from which the correlation factors have been derived are given in Table 7.1. The method is only suitable for leading-edge devices that extend to the wing tip.

5. EFFECTS OF MACH NUMBER AND REYNOLDS NUMBER

5.1 Mach Number Effects

High local Mach numbers will occur at low free-stream Mach number as a result of the deployment of high-lift devices. Mach number effects will occur at free-stream Mach numbers greater than about 0.2, depending on detailed section and leading-edge device geometry. None of the data considered for this Item was for a Mach number greater than 0.25. Reference 29 provides background information on the effects of Mach number but insufficient data were available from which to derive a comprehensive prediction method suitable for higher Mach numbers.

5.2 Reynolds Number Effects

Reynolds number effects are allowed for via the prediction of $\Delta C'_{Lml}$ in Item No. 94027. From the data used in the derivation of this Item no additional effects of Reynolds number were found. Reference 29 gives more detailed information on Reynolds number effects for some specific cases.

6. PREDICTION METHOD

Reports considered in the development of the method include Derivations 18, 19, 20, 22 and Reference 26. The main effects of aspect ratio, taper ratio and sweep on the spanwise loading are allowed for by the concepts used in Item No. 89034.

From Item No. 89034 for a plain wing with little or no sweep, where the effects of outboard flow of the boundary layer may be neglected, it is necessary to establish the spanwise variation of C_{LL} and to compare this with the spanwise variation of C_{Lm} , the maximum lift coefficient of the aerofoil section. For the incidence at which the peak local lift coefficient, C_{LLp} , matches the local section maximum lift coefficient, C_{Lm} , the distribution of C_{LL}/\bar{c} must be obtained and integrated to obtain the value of the maximum lift coefficient of the wing, C_{Lmax} . This concept is extended to apply to a wing with a full-span leading-edge device and hence for the increment in C_{Lmax} due to the device.

The same simplifying assumptions as those used in Item No. 89034 have been made to reduce the complex procedure outlined above to the calculation for only the most highly loaded spanwise station for loading due to incidence. The spanwise position, η_p , of this station and the corresponding normalised lift coefficient, μ_p , are shown in Figures 1 and 2, which are taken from Item No. 89034. These Figures are in terms of taper ratio, λ , and the spanwise centre of pressure location, $\bar{\eta}$, corresponding to the spanwise loading due to incidence, from Item No. 83040 (Derivation 2).

For wings with part-span leading-edge devices ΔC_{Lmaxl} is dependent on their spanwise location. Figure 3 is based on an analysis of data from Derivation 13, but there were insufficient data for a full determination of part-span effects. In the absence of more relevant information this may be used as a guide to part-span effects for cases where the leading-edge device extends to the wing tip. Maximum lift increments can be very much reduced if the outboard end of the leading-edge device is inboard of the wing tip, especially on swept wings where increments may be reduced to the order of 50% of their full-span value, even for η_{ol} greater than 0.9.

The effects of wing sweep have been derived from analysis of data from Derivations 13 to 15 and 23 to 25 and include the use of geometrical characteristics for the section normal to the leading edge at the spanwise location of maximum loading due to incidence (see Sketch 1.1), Reynolds number effects relating to the Reynolds number normal to the leading-edge, leading-edge device angles taken streamwise and a sweep correlation factor $K_{\Lambda l}$.

McRae (Derivation 19) and Torenbeek (Derivation 21) noted that the combination of slotted leading- and trailing-edge devices on a wing produces a smaller increment in lift than the sum of the two independent effects. McRae identified gross thickening of the combined slat wake and main flap element boundary layer as the probable reason for this. The prediction method includes an empirical allowance for this effect based on correlation of the data. The extent of this effect is dependent on slat gap size and is reflected in the different values of K_l for slats from Item No. 94027 compared to those given in Item Nos 94030 and 94031, for aerofoils without and with deployed slotted trailing-edge flaps.

6.1 General Expression

Equation (3.12) of Item No. 94027 gives the general expression for the increment in maximum lift coefficient due to deployment of a leading-edge device on an aerofoil for the datum Reynolds number based on c of 3.5×10^6 as:

$$\Delta C_{L_{ml}} = (c'/c)\Delta C'_{L_{ml}} \quad (6.1)$$

where $\Delta C'_{L_{ml}}$ is the increment in the aerofoil maximum lift coefficient due to a leading-edge device, based on the extended chord and derived from Item No. 94027 for a Reynolds number of 3.5×10^6 for given aerofoil and leading-edge device geometry at the section $\eta = \eta_p$.

The general expression for the maximum lift coefficient of a wing with both leading-edge devices and trailing-edge flaps deployed is:

$$C_{L_{max}} = C_{L_{maxB}} + \Delta C_{L_{max}} \quad (6.2)$$

where $\Delta C_{L_{max}} = \Delta C_{L_{maxl}} + \Delta C_{L_{maxt}}$. (6.3)

Here $C_{L_{maxB}}$ is the maximum lift coefficient of the basic wing (*i.e.* without high-lift devices deployed) and is obtained from Item No. 89034,

$\Delta C_{L_{maxt}}$ is the increment in wing maximum lift coefficient due to deployment of trailing-edge flaps and is obtained from Item No. 91014,

and $\Delta C_{L_{maxl}}$ is the increment in wing maximum lift coefficient due to deployment of leading-edge high-lift devices extending to the wing tip, with or without trailing-edge flap deployment, see Sections 6.2 and 6.3 for unswept and swept wings.

6.2 Unswept Wings

For an unswept wing:

$$\Delta C_{L_{maxl}} = F_R(\Delta C_{L_{ml}}/\mu_p)\psi_i \quad (6.4)$$

where, from Item No. 94027,

$$F_R = 0.153 \log_{10} R_{cp} \quad (6.5)$$

allows for the effect of Reynolds number variation on the high-lift devices and ΔC_{Lml} is obtained from Equation (6.1). As noted earlier, if a slotted leading-edge device is deployed in combination with a slotted trailing-edge flap then the value of ΔC_{Lml} is rather less than that with the flap undeployed, see Item No 94030 or 94031.

The denominator μ_p in Equation (6.4) is the ratio of the peak local lift coefficient to the wing lift coefficient, C_{LLp}/C_L , for the loading due to incidence and is obtained from Figure 2 as a function of λ and $\bar{\eta}$. The part-span factor ψ_i for leading-edge devices extending to the wing tip is obtained from Figure 3 as a function of η_{il} .

6.3 Swept Wings

For a swept wing (*i.e.* $\Lambda_{1/4} > 5^\circ$, say) the increment in wing maximum lift coefficient due to the deployment of leading-edge high-lift devices extending to the wing tip is:

$$\Delta C_{Lmaxl} = F_R K_{\Lambda l} (\Delta C_{Lml} / \mu_p) \psi_i \quad (6.6)$$

where
$$F_R = 0.153 \log_{10} (R_{cp} \cos^2 \Lambda_0), \quad (6.7)$$

allows for the effect of Reynolds number variation on the high-lift device,

and $K_{\Lambda l}$ is a factor to allow for the effect of wing sweep on the increment in the maximum lift coefficient due to a leading-edge device and is taken to be

$$K_{\Lambda l} = \cos \Lambda_{1/4}. \quad (6.8)$$

The parameter ΔC_{Lml} is obtained from Equation (6.1) and in deriving $\Delta C'_{Lml}$ the relevant section geometry parameters are taken normal to the leading edge at η_p , so that when using Figures 1 and 2 of Item No. 94027 the following approximate substitutions are made:

replace ρ_l/c	with	$(\rho_l/c) \sec \Lambda_0^*$
replace G_l/c	with	$(G_l/c) \sec \Lambda_0$
replace H_l/c	with	$(H_l/c) \sec \Lambda_0$.

Empirical analysis of the available test data showed that the leading-edge device deflection angle requires special consideration for swept wings. In the determination of K_l from Figures 1a to 1c of Item No. 94027 (or, for combined slotted leading-edge devices and trailing-edge flaps, Figure 5 of Item No. 94030 and Figure 10 of Item No. 94031) δ_l° is replaced with $\delta_l^\circ \cos \Lambda_0$. However, in the evaluation of Equation (3.10) for $\Delta C'_{Lml}$ in Item No. 94027 the streamwise value of δ_l is retained.

As described in Section 6.2, the values of μ_p and ψ_i are obtained from Figures 2 and 3 respectively.

* Attempts to correlate the data using $(\rho_l/c) \sec^2 \Lambda_0$ with leading-edge flap angles taken chordwise were unsuccessful.

7. APPLICABILITY AND ACCURACY

7.1 Applicability

The method given in this Item for estimating the increment in maximum lift coefficient due to deployment of leading-edge high-lift devices on a wing with or without trailing-edge flaps deployed is applicable to straight-tapered wings for the range of wing planform parameters shown in Table 7.1. All wings used in the derivation of the Item had either a smooth surface or a narrow band of roughness near the leading edge with height just sufficient to ensure boundary-layer transition.

It should be noted that the performance of leading-edge devices can be quite sensitive to detail design. For example, variation in the slot geometry via the shape of the lower surface of the slat and the leading-edge shape of the fixed part of the wing can change C_{Lmax} by up to 70% of ΔC_{Lmax} and supporting structures can also cause reduction in C_{Lmax} due to extensive flow separations.

For wings with cranked leading or trailing edges or curved tips it is suggested that the calculation of ΔC_{Lmax} , in Equations (6.4) and (6.6) be made for the equivalent straight-tapered planform as defined in Item No. 76003 (Derivation 1).

Data correlation has included the following range of parameters.

TABLE 7.1

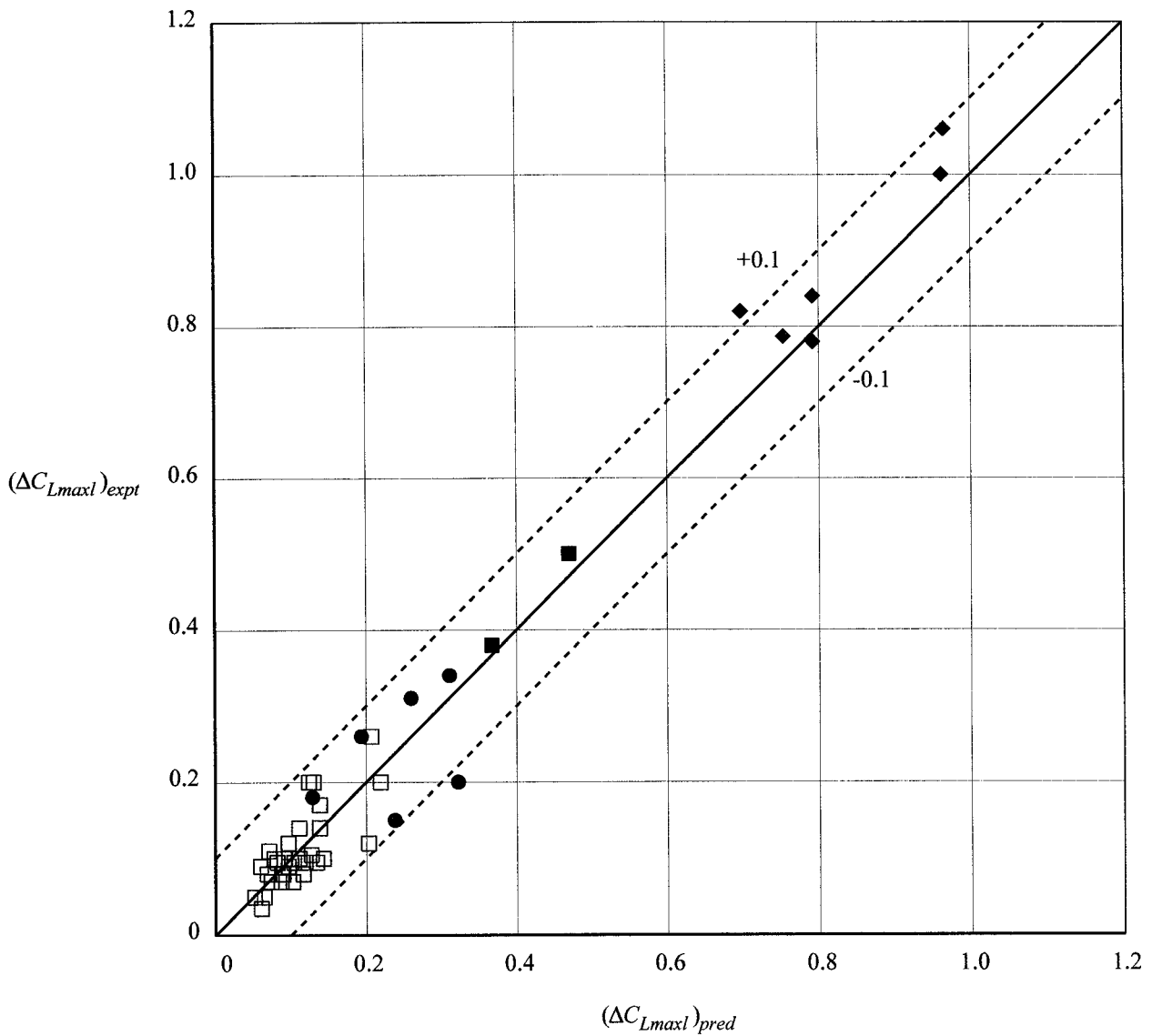
<i>Parameter</i>	<i>Range</i>
A	2.6 to 8.4
Λ_0	0 to 47°
Λ_1	0 to 43°
λ	0.25 to 1.0
$A \tan \Lambda_0$	0 to 5.6
η_{il}	0 to 0.7
η_{ol}	1.0*
Λ_{hl}	0 to 46°
$R_c \times 10^{-6}$	0.7 to 7
M	≤ 0.25

* Note that the method is unsuitable unless the leading-edge device extends to the wing tip, *i.e.* $\eta_{ol} = 1$ see Section 6.

7.2 Accuracy

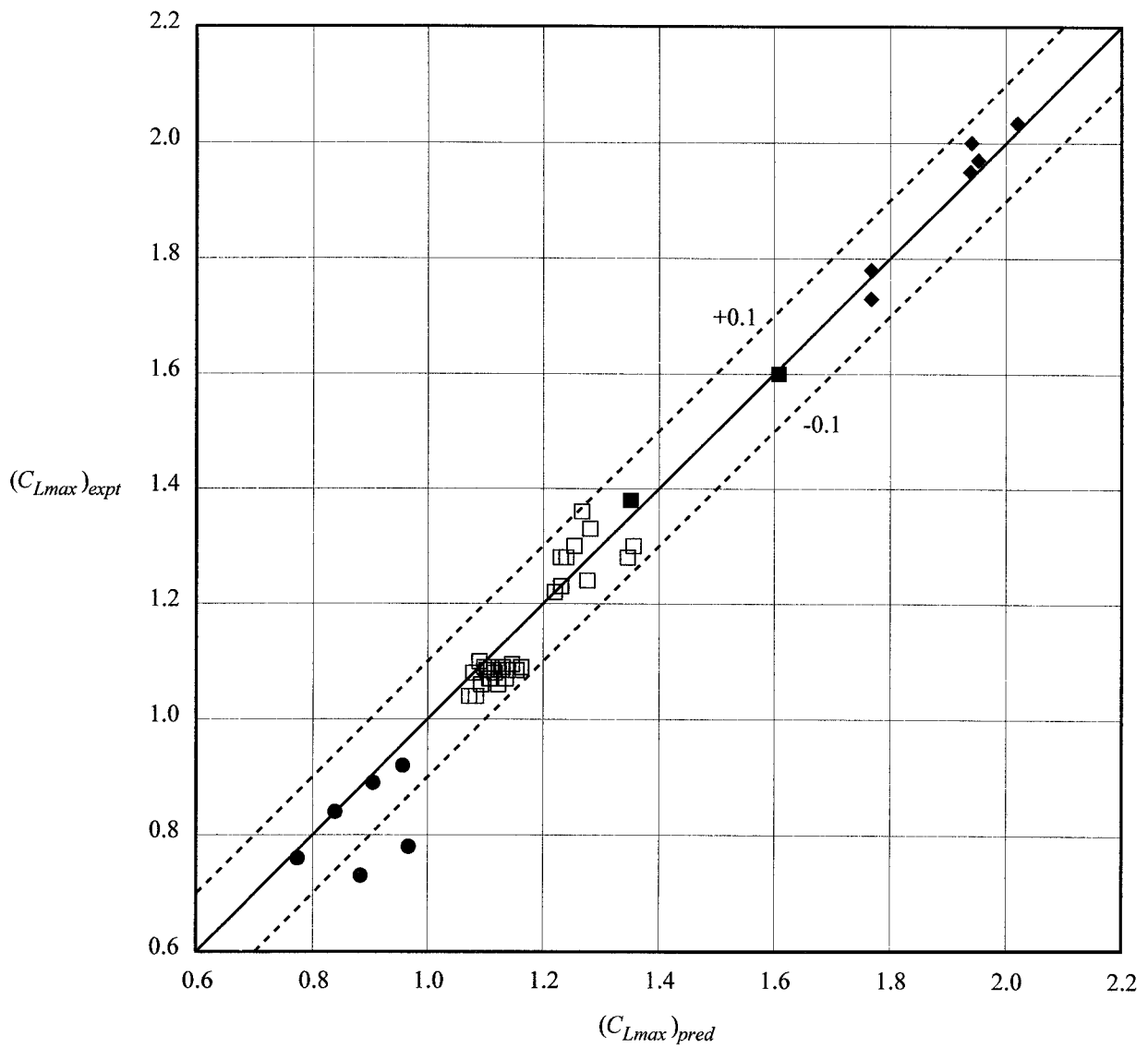
Sketch 7.1 shows the comparison between experimental and predicted values of the increment in maximum lift coefficient due to leading-edge device deployment on a wing without trailing-edge devices. Sketch 7.2 shows the comparison of the total maximum lift coefficient, where C_{Lmax} for the plain wing was obtained using Item No. 89034. Sketch 7.3 shows the corresponding comparison between experimental and predicted values of the increment in maximum lift coefficient due to leading-edge device deployment on a wing with trailing-edge flaps deployed. Sketch 7.4 shows the comparison for the combined effect on maximum lift coefficient of leading-edge device and trailing-edge flap deployment. Finally, Sketch 7.5 shows the comparison between experimental and predicted values of the total maximum lift coefficient, with leading-edge devices and trailing-edge flaps deployed, where the maximum lift coefficient of the plain wing was obtained using Item No. 89034. The experimental data were obtained from Derivations 12 to 17, 23 to 25 and Reference 28. The overall accuracy of the predictions is generally within about ± 0.1 for ΔC_{Lmax} , ΔC_{Lmax} , and C_{Lmax} .

<i>Leading-edge Device:</i>		
<i>Type</i>	<i>Full Span</i>	<i>Part Span</i>
Plain flap/Droop	●	
Slat	◆	
Krüger	■	□



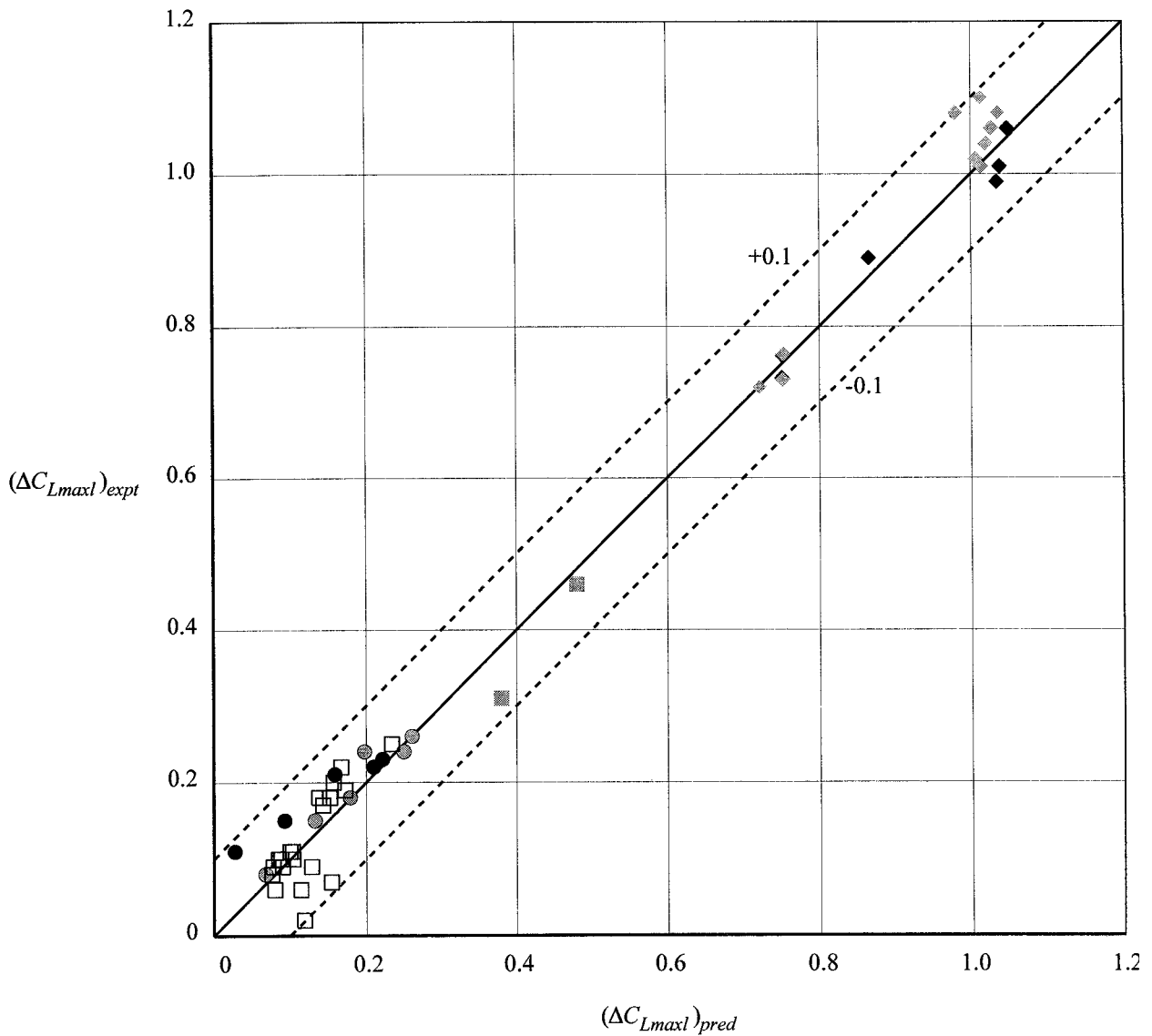
Sketch 7.1 Correlation of ΔC_{Lmaxl} without trailing-edge flaps

<i>Leading - edge Device:</i>		
<i>Type</i>	<i>Full Span</i>	<i>Part Span</i>
Plain flap/Droop	●	
Slat	◆	
Krüger	■	□



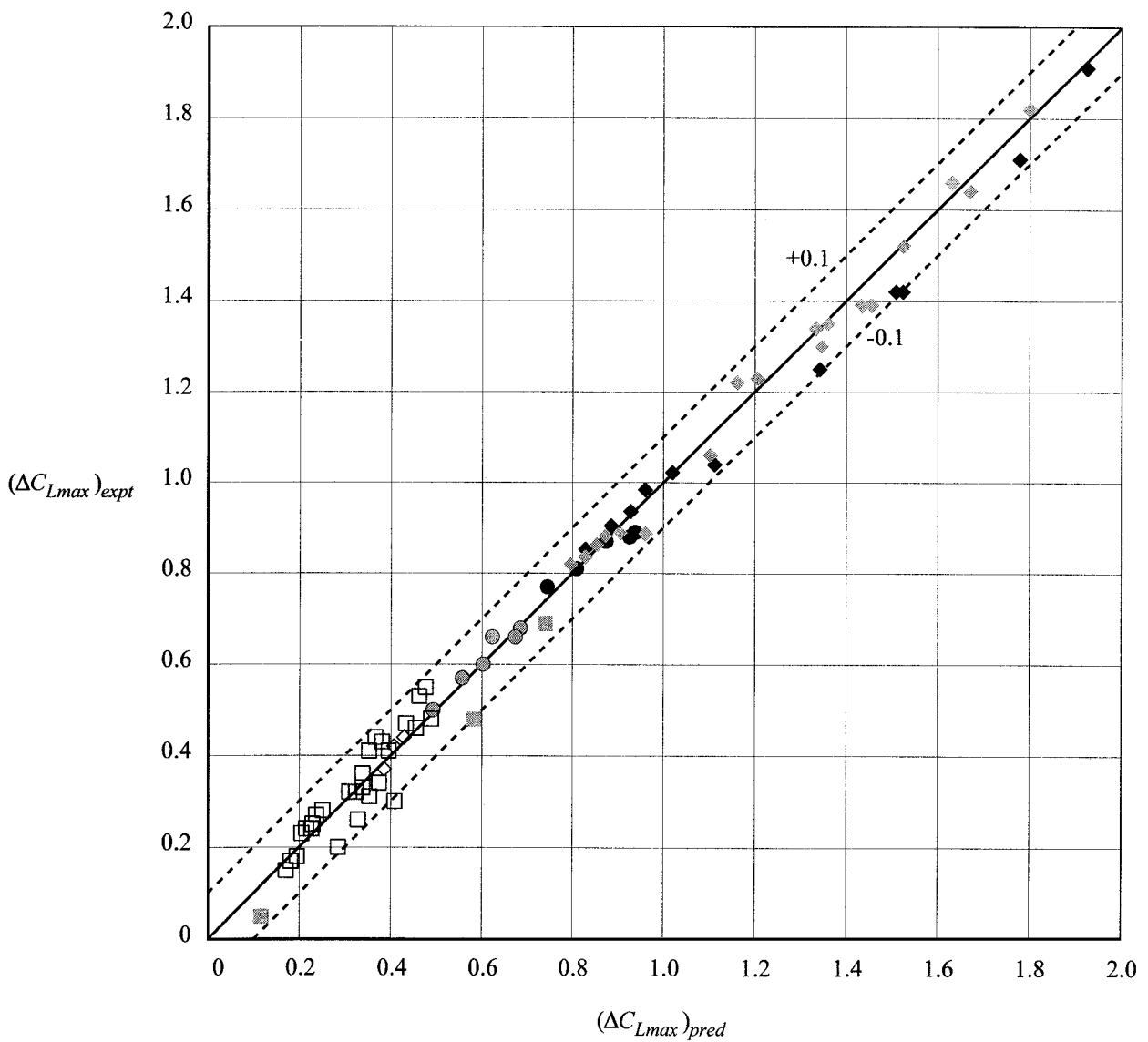
Sketch 7.2 Correlation of C_{Lmax} for wings with leading-edge devices deployed

<i>Leading - edge Device:</i>				
<i>Type</i>	<i>Full Span</i>		<i>Part Span</i>	
	<i>Trailing - edge Flap:</i>			
	<i>Full Span</i>	<i>Part Span</i>	<i>Full Span</i>	<i>Part Span</i>
Plain flap/Droop	●	⊙		
Slat	◆	◊		
Krüger		■		□



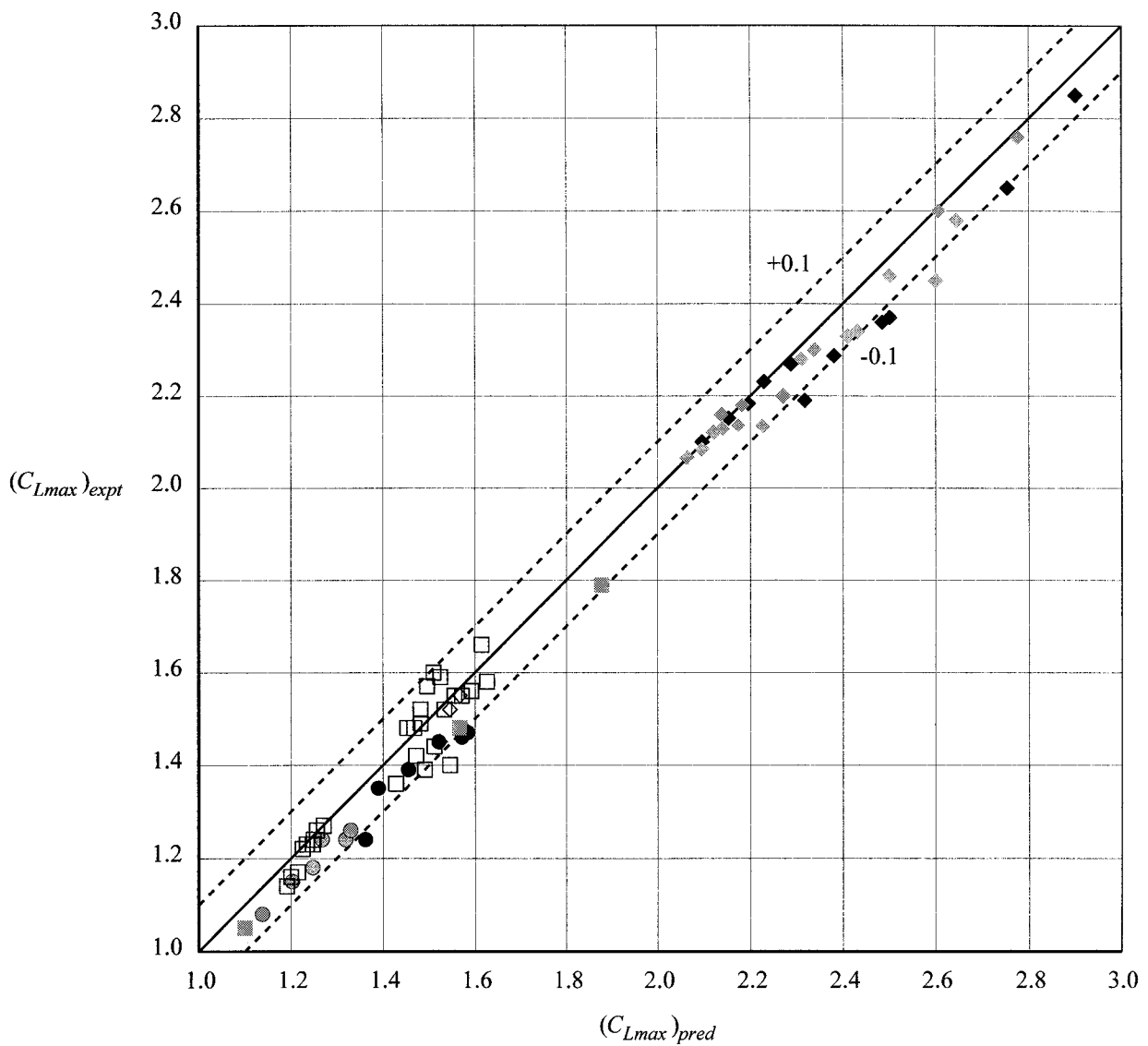
Sketch 7.3 Correlation of ΔC_{Lmaxl} for wings with trailing-edge flaps deployed

<i>Leading - edge Device:</i>				
<i>Type</i>	<i>Full Span</i>		<i>Part Span</i>	
	<i>Trailing - edge Flap:</i>			
	<i>Full Span</i>	<i>Part Span</i>	<i>Full Span</i>	<i>Part Span</i>
Plain flap/Droop	●	⊙		
Slat	◆	◇		◇
Krüger		■		□



Sketch 7.4 Correlation of ΔC_{Lmax} due to deployment of leading-edge and trailing-edge devices

<i>Leading - edge Device:</i>				
<i>Type</i>	<i>Full Span</i>		<i>Part Span</i>	
<i>Plain flap/Droop</i>	<i>Trailing - edge Flap:</i>			
	<i>Full Span</i>	<i>Part Span</i>	<i>Full Span</i>	<i>Part Span</i>
	●	⊙		
	◆	◇		◇
<i>Slat</i>		◆		◇
<i>Krüger</i>		■		□



Sketch 7.5 Correlation of C_{Lmax} for wings with leading-edge and trailing-edge devices deployed

8. DERIVATION AND REFERENCES

8.1 Derivation

The Derivation lists selected sources of information that have assisted in the preparation of this Item.

8.1.1 ESDU Data Items

1. ESDU Geometric properties of cranked and straight tapered wing planforms. ESDU International, Item No. 76003, 1976.
2. ESDU Method for the rapid estimation of spanwise loading of wings with camber and twist in subsonic attached flow. ESDU International, Item No. 83040, 1983.
3. ESDU Aerofoil maximum lift coefficient for Mach numbers up to 0.4. ESDU International, Item No. 84026, 1984.
4. ESDU The maximum lift coefficient of plain wings at subsonic speeds. ESDU International, Item No. 89034, 1989.
5. ESDU Maximum lift of wings with trailing-edge flaps at low speeds. ESDU International, Item No. 91014, 1991.
6. ESDU Introduction to the estimation of the lift coefficients at zero angle of attack and at maximum lift for aerofoils with high-lift devices at low speeds. ESDU International, Item No. 94026, 1994.
7. ESDU Increments in aerofoil lift coefficient at zero angle of attack and in maximum lift coefficient due to deployment of various leading-edge high-lift devices at low speeds. ESDU International, Item No. 94027, 1994.
8. ESDU Increments in aerofoil lift coefficient at zero angle of attack in maximum lift coefficient due to deployment of a plain trailing-edge flap, with or without a leading-edge high-lift device, at low speeds. ESDU International, Item No. 94028, 1994.
9. ESDU Increments in aerofoil lift coefficient at zero angle of attack and in maximum lift coefficient due to deployment of a trailing-edge split flap, with or without a leading-edge high-lift device, at low speeds. ESDU International, Item No. 94029, 1994.
10. ESDU Increments in aerofoil lift coefficient at zero angle of attack and in maximum lift coefficient due to deployment of a single-slotted trailing-edge flap, with or without a leading-edge high-lift device, at low speeds. ESDU International, Item No. 94030, 1995.
11. ESDU Increments in aerofoil lift coefficient at zero angle of attack and in maximum lift coefficient due to deployment of a double-slotted or triple-slotted trailing-edge flap, with or without a leading-edge high-lift device, at low speeds. ESDU International, Item No. 94031, 1995.

8.1.2 Wind-tunnel test reports

12. CONNER, D.W.
NEELY, R.H. Effects of a fuselage and various stall control flaps on aerodynamic characteristics in pitch of a NACA 64-series 40° swept-back wing. NACA RM L6L27 (TIL 1375), 1947.
13. GRAHAM, R.R.
CONNER, D.W. Investigation of high lift and stall-control devices on a NACA 64-series 42° sweptback wing with and without fuselage. NACA RM L7G09 (TIL 1407), 1947.
14. LICHTENSTEIN, J.H. Effect of high-lift devices on the low speed static lateral and yawing stability characteristics of an untapered 45° sweptback wing. NACA tech. Note 2689, 1948.
15. LANGE, R.H.
MAY, R.W. Effect of leading-edge high lift devices and split flaps on the maximum lift and lateral characteristics of a rectangular wing of aspect ratio 3.4 with circular arc airfoil sections at Reynolds numbers from 2.9×10^6 to 8.4×10^6 . NACA RM L8D30 (TIL 1971), 1948.
16. PASAMANICK, J.
SELLERS, T.B. Low speed investigation of leading-edge and trailing-edge flaps on a 47.5° sweptback wing of aspect ratio 3.4. NACA RM L50E02 (TIL 2404), 1950.
17. SALMI, R.J. Effects of leading-edge device and trailing-edge flaps on longitudinal characteristics of two 47.7° sweptback wings of aspect ratio 5.1 and 6 at a Reynolds number of 6.0×10^6 . NACA RM L50F20 (TIL 2466), 1950.
18. ROSHKO, A. Computation of the increment of maximum lift due to flaps. Douglas Report No. SM-23626, 1959.
19. McRAE, D.M. The aerodynamics of high-lift devices on conventional aircraft. *Aeronaut. J.*, Vol. 73, pp.535-541, June 1969.
20. SANDERS, K.L. High lift devices, a weight and performance tradeoff methodology. Ryan Aeronautical Company, Technical Paper No. 761, 1969.
21. TORENBEEK, E. *Synthesis of Subsonic Airplane Design*. Delft University Press, 1976.
22. BAC Unpublished data, 1973.
23. LOVELL, D.A. A wind tunnel investigation of the effects of flap span and deflection angle, wing planform and a body on the high lift performance of a 28° swept wing. RAE tech. Rep. 76030, 1976.
24. RAE Unpublished data, 1978.
25. RAE Unpublished data, 1981.

8.2 References

The References provide sources of information supplementary to that given in this Item.

- 26. YOUNG, A.D. The aerodynamic characteristics of flaps.
ARC R&M 2622, 1953.
- 27. SMITH, A.M.O. High-lift aerodynamics.
J. Aircr., Vol. 12, No. 6, pp.501 to 530, June 1975.
- 28. WOODWARD, D.S. Some wind tunnel measurements of the effectiveness at low speeds of
KEATING, R.F.A. combined lift and roll controls.
Paper No. 4 in Agard CP 262, Aerodynamic characteristics of controls,
1979.
- 29. FIDDES, S.P. Investigations into the effects of scale and compressibility on lift and
KIRBY, D.A. drag in the RAE 5m pressurised low-speed wind-tunnel. *Aeronaut. J.*,
WOODWARD, D.S. Vol. 89, pp.93 to 108, March 1985.
PECKHAM, D.H.

9. EXAMPLES

9.1 Example 1

Estimate the increment in maximum lift coefficient for a wing with a leading-edge slat for a Reynolds number $R_{\bar{c}} = 7 \times 10^6$ and a free-stream Mach number $M = 0.2$.

The wing has planform geometry parameters

$$A = 8, \Lambda_{1/4} = 25^\circ \text{ and } \lambda = 0.4$$

and a constant section, NACA 63₁-212, across the span for which

$$t/c = 0.12 \text{ and } \rho_l/c = 0.01087.$$

The slat has streamwise section geometry

$$\begin{array}{ll} \delta_l^\circ = 30.5^\circ, \text{ i.e. } \delta_l = 0.532 \text{ rad.} & H_l/c = 0.022 \\ c_l/c = 0.15 & L_l/c = 0.010 \\ x_l/c = 0.1405 & G_l/c = 0.012 \\ x_n/c = 0.03 & \end{array}$$

and extends from 15% semi-span ($\eta_{il} = 0.15$) to the wing tip ($\eta_{ol} = 1$).

There is no trailing-edge flap so that $\Delta c_t = 0$.

1. Check that the sweep angles are within the range of applicability of the method

From the relationships for planform geometry given in Item No. 76003,

$$\begin{aligned}\Lambda_0 &= \tan^{-1} \left[\tan \Lambda_{1/4} + \frac{1}{A} \left(\frac{1-\lambda}{1+\lambda} \right) \right] \\ &= \tan^{-1} \left[\tan 25^\circ + \frac{1}{8} \left(\frac{1-0.4}{1+0.4} \right) \right] \\ &= 27.5^\circ.\end{aligned}$$

$$\begin{aligned}\Lambda_1 &= \tan^{-1} \left[\tan \Lambda_{1/4} - \frac{3}{A} \left(\frac{1-\lambda}{1+\lambda} \right) \right] \\ &= \tan^{-1} \left[\tan 25^\circ - \frac{3}{8} \left(\frac{1-0.4}{1+0.4} \right) \right] \\ &= 17.0^\circ.\end{aligned}$$

The hinge-line sweep angle, Λ_{hl} , is that of the 0.1405 chord line, *i.e.*

$$\begin{aligned}\Lambda_{hl} &= \tan^{-1} \left[\tan \Lambda_{1/4} + \frac{4}{A} \left(\frac{1}{4} - 0.1405 \right) \left(\frac{1-\lambda}{1+\lambda} \right) \right] \\ &= 26.1^\circ.\end{aligned}$$

From Table 7.1 it is seen that the values of Λ_0 , Λ_1 and Λ_{hl} all lie within the permitted ranges.

2. Determine the required wing planform parameters

From the relationship in Item No. 76003, with the given values of A , $\Lambda_{1/4}$ and λ

$$\begin{aligned}A \tan \Lambda_{1/2} &= A \tan \Lambda_{1/4} - \frac{1-\lambda}{1+\lambda} \\ &= 8 \times \tan 25^\circ - \frac{1-0.4}{1+0.4} \\ &= 3.302.\end{aligned}$$

The wing taper parameter κ is given by

$$\begin{aligned}\kappa &= \frac{1+2\lambda}{3(1+\lambda)} \\ &= \frac{1+2 \times 0.4}{3(1+0.4)} \\ &= 0.429.\end{aligned}$$

3. Determine $\bar{\eta}$ from Item No. 83040

Since $M = 0.2$,

$$\begin{aligned}\beta A &= (1 - M^2)^{1/2} A \\ &= (1 - 0.2^2)^{1/2} \times 8 \\ &= 7.84,\end{aligned}$$

and so with $A \tan \Lambda_{1/2} = 3.302$ and $\kappa = 0.429$ a cross-plot in βA using Figures 1 to 5 of Item No. 83040 gives

$$\bar{\eta} = 0.437.$$

4. Determine η_p

From Figure 1, with $\bar{\eta} = 0.437$ and $\lambda = 0.4$,

$$\eta_p = 0.69.$$

5. Determine μ_p

From Figure 2, with $\bar{\eta} = 0.437$ and $\lambda = 0.4$,

$$\mu_p = 1.15.$$

6. Determine $R_{cp} \cos^2 \Lambda_0$ appropriate to η_p

For $\kappa = 0.4$, and $\eta_p = 0.69$ the streamwise chord c_p at η_p is given by

$$\begin{aligned}c_p / \bar{c} &= \frac{3}{2} \left[\frac{1 + \lambda}{1 + \lambda + \lambda^2} \right] (1 - \eta_p + \lambda \eta_p) \\ &= \frac{3}{2} \left[\frac{1 + 0.4}{1 + 0.4 + 0.4^2} \right] (1 - 0.69 + 0.4 \times 0.69) \\ &= 0.7888.\end{aligned}$$

The Reynolds number at η_p is given by

$$\begin{aligned}R_{cp} &= R_{\bar{c}} \times c_p / \bar{c} \\ &= 7 \times 10^6 \times 0.7888 \\ &= 5.522 \times 10^6.\end{aligned}$$

Hence

$$\begin{aligned} R_{cp} \cos^2 \Lambda_0 &= 5.522 \times 10^6 \times \cos^2(27.5^\circ) \\ &= 4.345 \times 10^6 . \end{aligned}$$

7. Determine ΔC_{Lml} using Item No. 94027

For use in Item No. 94027 the following parameters are required:

$$\begin{aligned} (\rho_l/c) \sec \Lambda_0 &= 0.01087 \times \sec(27.5^\circ) \\ &= 0.0123. \end{aligned}$$

From Equation (4.4a) of Item No. 94027, with allowance for a trailing-edge flap,

$$\begin{aligned} c'/c &= 1 + c_l/c - x_n/c - L_l/c - (H_l/c) \tan(\delta_l^\circ/2) + \Delta c_t/c \\ &= 1 + 0.15 - 0.03 - 0.010 - 0.022 \times \tan(30.5^\circ/2) + 0 \\ &= 1.104. \end{aligned}$$

Table 4.1 of Item No. 94027 shows that the value of c_{el} is taken as c_l for a slat, *i.e.*

$$c_{el}/c = c_l/c = 0.15 .$$

Therefore

$$\begin{aligned} c_{el}/c' &= (c_{el}/c)/(c'/c) \\ &= 0.15/1.104 \\ &= 0.1359. \end{aligned}$$

Figure 3 of Item No. 94027, with a slat dimensionless overlap of

$$\begin{aligned} L_l/(x_l - x_n) &= (L_l/c)/(x_l/c - x_n/c) \\ &= 0.01/(0.1405 - 0.03) \\ &= 0.090, \end{aligned}$$

gives $K_e = 0.995$.

For $(\rho_l/c) \sec \Lambda_0 = 0.0123$, Figure 2b of Item No. 94027 gives

$$K_g = 1.41$$

and for $\delta_l^\circ \cos \Lambda_0 = 30.5^\circ \times \cos(25^\circ)$

$$= 27.64^\circ$$

and $(G_l/c) \sec \Lambda_0 = 0.012 \times \sec(25^\circ)$

$$= 0.013,$$

Figure 1b of Item No. 94027 gives

$$K_l = 0.97.$$

Therefore, Equation (3.10) of Item No. 94027 gives (with $\delta_0 = 0.25$ for a slat, from Table 4.1 of that Item)

$$\begin{aligned} \Delta C'_{Lmt} &= 2K_e K_g K_l (\delta_l - \delta_0) [1 - (1 - 2c_{el}/c')^2]^{1/2} \\ &= 2 \times 0.995 \times 1.41 \times 0.97 \times (0.532 - 0.25) \times [1 - (1 - 2 \times 0.1359)^2]^{1/2} \\ &= 0.5260. \end{aligned}$$

From Equation (6.1),

$$\begin{aligned} \Delta C_{Lml} &= (c'/c) \Delta C'_{Lml} \\ &= 1.104 \times 0.5260 \\ &= 0.5807. \end{aligned}$$

8. Determine ψ_i

From Figure 3, for $\eta_{il} = 0.15$,

$$\psi_i = 0.73.$$

9. Determine ΔC_{Lmaxl}

From Equation (6.6)

$$\Delta C_{Lmaxl} = F_R K_{\Lambda l} (\Delta C_{Lml} / \mu_p) \psi_i,$$

where, from Equation (6.7),

$$\begin{aligned}
 F_R &= 0.153 \log_{10}(R_{cp} \cos^2 \Lambda_0) \\
 &= 0.153 \log_{10}(4.345 \times 10^6) \\
 &= 1.0156,
 \end{aligned}$$

and, from Equation (6.8)

$$\begin{aligned}
 K_{\Lambda l} &= \cos \Lambda_{1/4} \\
 &= \cos(25^\circ) \\
 &= 0.9063.
 \end{aligned}$$

Therefore

$$\begin{aligned}
 \Delta C_{Lmaxl} &= 1.0156 \times 0.9063 \times (0.5807 / 1.15) \times 0.73 \\
 &= 0.339.
 \end{aligned}$$

9.2 Example 2

For the same wing, slat and flow conditions as in Example 1 estimate the increment in maximum lift coefficient due to the deployed combination of leading-edge slat and a plain trailing-edge flap.

The relevant flap geometry parameters are:

Plain flap with $c_t/c = 0.3$, $\delta_t^\circ = 35^\circ$ and $\phi_t^\circ = 7.7^\circ$,

extending from 15% semi-span ($\eta_{it} = 0.15$) to 60% semi-span ($\eta_{ot} = 0.6$).

1. Determine ΔC_{Lmaxl}

From Equation (3.10) of Item No. 94027 the only influence of a trailing-edge flap on $\Delta C'_{Lml}$ results from any increase of chord, c' , due to extension of the flap and from any change in K_l . A further influence on ΔC_{Lml} arises from the effect of any increase in c' via Equation (6.1). However, for a plain flap, firstly there is no change to c' , because $\Delta c_t = 0$, and secondly the value of K_l is the same as for the case with flap undeflected because it is only for slotted flap deployment that K_l is affected, see Section 6.3. In the present case, therefore, there is no change to the calculation procedure for ΔC_{Lml} and so from Example 1

$$\Delta C_{Lml} = 0.339.$$

2. Determine ΔC_{Lmaxt}

The wing and the trailing-edge flap are the same (except for the changed value of η_{it}) as in the Example of Item No. 91014. The procedure of that Item is therefore followed, but with due allowances for the increase in chord arising from slat deployment and the increase in η_{it} . Rather than repeat all the intermediate calculations, a list of the values of those parameters that are modified by the increase in chord is given as a check. In the notation of Item No. 91014, they are

$c_t/c' = 0.272$, $C'_{L0t} = 1.146$, $T = 0.403$ (for $x'_s/c' = \frac{1}{2}c_{el}/c' = 0.068$, see Section 4.2 of Item No. 94028, and $c_t/c' = 0.272$), $\Delta C'_{Lmt} = 0.604$, $\Delta C_{Lmt} = 0.667$.

The changed value of $\eta_{it} = 0.15$ gives $\Phi_i = 0.21$.

These modified values lead to

$$\Delta C_{Lmaxt} = 0.235.$$

3. Determine ΔC_{Lmax}

From Equation (6.3)

$$\begin{aligned}\Delta C_{Lmax} &= \Delta C_{Lmaxl} + \Delta C_{Lmaxt} \\ &= 0.339 + 0.235 \\ &= 0.574.\end{aligned}$$

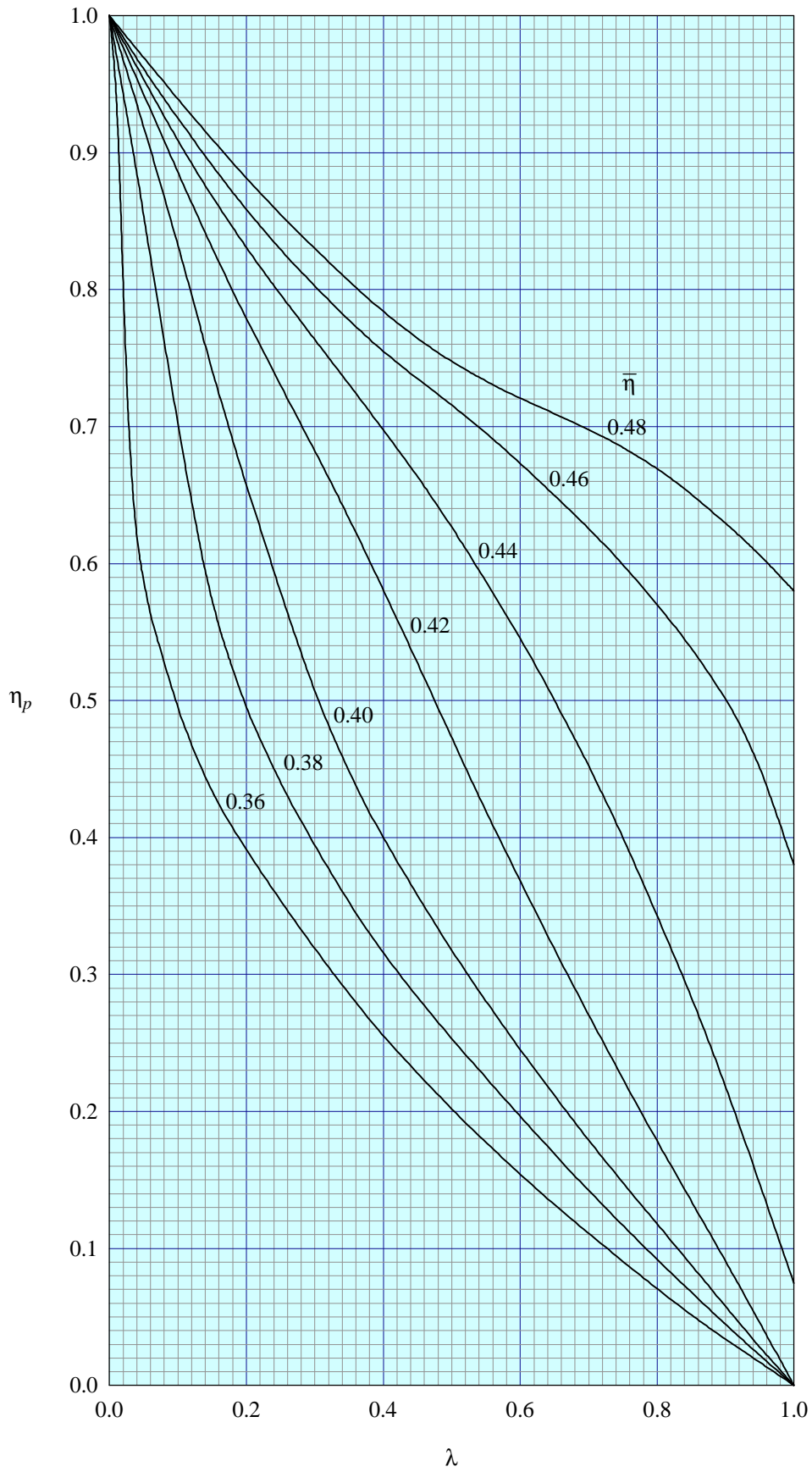


FIGURE 1 VARIATION OF η_p WITH λ AND $\bar{\eta}$

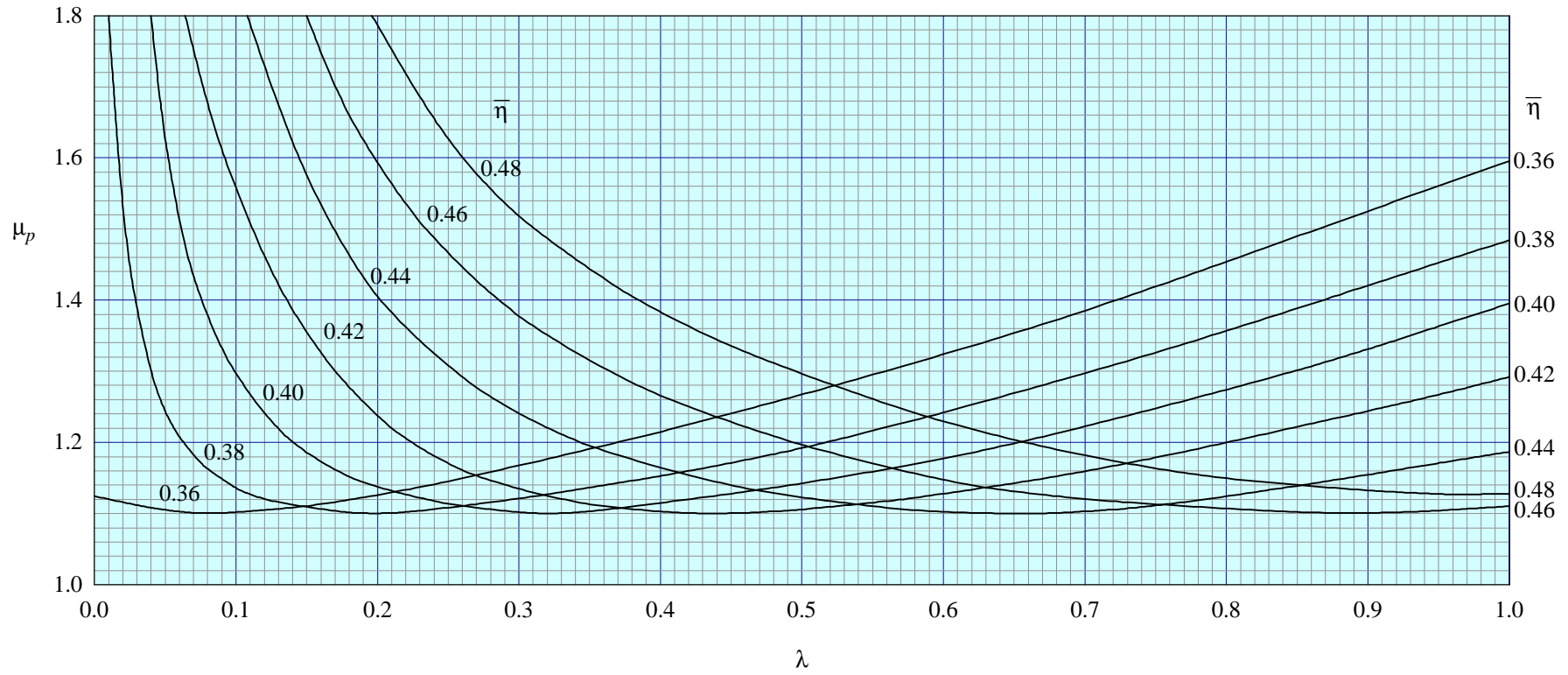


FIGURE 2 VARIATION OF μ_p WITH λ AND $\bar{\eta}$

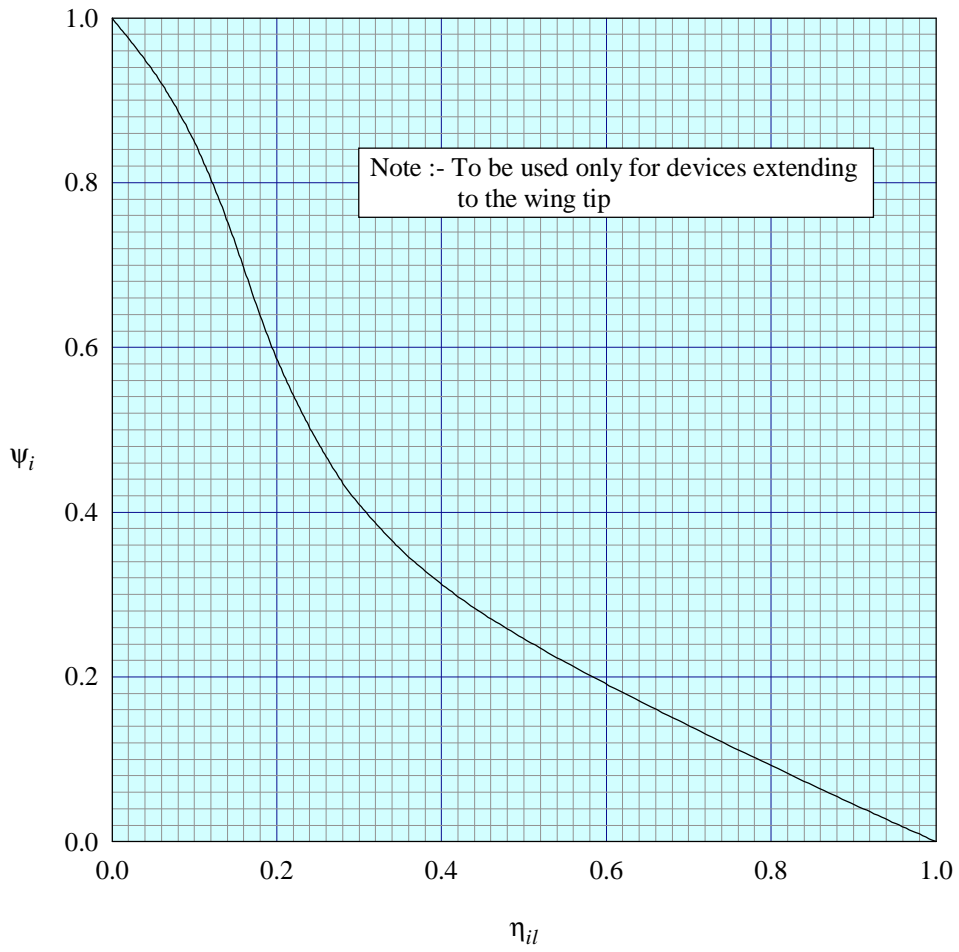


FIGURE 3 PART-SPAN FACTOR FOR LEADING-EDGE DEVICES

THE PREPARATION OF THIS DATA ITEM

The work on this particular Item was monitored and guided by the Aerodynamics Committee which first met in 1942 and now has the following membership:

Chairman

Mr H.C. Garner – Independent

Members

Mr G.E. Bean* – Boeing Commercial Airplane Company, Seattle, Wash., USA

Dr P.C. Dexter – British Aerospace plc, Sowerby Research Centre, Bristol

Mr J.R.J. Dovey – Independent

Dr K.P. Garry – Cranfield University

Mr D.H. Graham* – Northrop Grumman Corp., Pico Rivera, Calif., USA

Mr M.J. Green – Avro International Aerospace Ltd, Woodford

Dr H.P. Horton – Queen Mary and Westfield College, University of London

Dr D.W. Hurst – University of Southampton

Mr P.K. Jones – Independent

Mr K. Karling* – Saab-Scania AB, Linköping, Sweden

Dr E.H. Kitchen – Rolls-Royce plc, Derby

Mr M. Maurel – Aérospatiale, Toulouse, France

Mr C.M. Newbold – Aircraft Research Association, Bedford

Mr J.B. Newton – British Aerospace Defence Ltd, Warton

Mr R. Sanderson – Daimler-Benz Aerospace Airbus GmbH, Bremen, Germany

Mr A.E. Sewell* – McDonnell Douglas Aerospace, Long Beach, Calif., USA

Mr J. Tweedie – Short Brothers plc, Belfast.

* Corresponding Member

The technical work in the assessment of the available information and the construction and subsequent development of the Data Item was carried out under contract to ESDU by Mr J.R.J. Dovey.